coatings

MDPI

Article

Nondestructive Evaluation of Thermal Barrier Coatings Interface Delamination Using Terahertz Technique Combined with SWT-PCA-GA-BP Algorithm

Dongdong Ye, Weize Wang *, Changdong Yin, Zhou Xu, Huanjie Fang, Jibo Huang and Yuanjun Li

Key Lab of Safety Science of Pressurized System, Ministry of Education, School of Mechanical and Power Engineering, East China University of Science and Technology, Shanghai 200237, China; Y10170088@mail.ecust.edu.cn (D.Y.); Y30180365@mail.ecust.edu.cn (C.Y.); Y45180021@mail.ecust.edu.cn (Z.X.); Y12190033@mail.ecust.edu.cn (H.F.); Y20150084@mail.ecust.edu.cn (J.H.); Y45180131@mail.ecust.edu.cn (Y.L.)

* Correspondence: wangwz@ecust.edu.cn; Tel.: +86-21-64252819; Fax: +86-21-64253513

Received: 14 August 2020; Accepted: 2 September 2020; Published: 4 September 2020



Abstract: Thermal barrier coatings (TBCs) are usually subjected to the combined action of compressive stress, tensile stress, and bending shear stress, resulting in the interfacial delamination of TBCs, and finally causing the ceramic top coat to peel off. Hence, it is vital to detect the early-stage subcritical delamination cracks. In this study, a novel hybrid artificial neural network combined with the terahertz nondestructive technology was presented to predict the thickness of interface delamination in the early stage. The finite difference time domain (FDTD) algorithm was used to obtain the raw terahertz time-domain signals of 32 TBCs samples with various thicknesses of interface delamination, not only that, the influence of roughness and the thickness of the ceramic top layer were considered comprehensively when modeling. The stationary wavelet transform (SWT) and principal component analysis (PCA) methods were employed to extract the signal features and reduce the data dimensions before modeling, to make the cumulative contribution rate reach 100%, the first 31 components of the SWT detail data was used as the input data during modeling. Finally, a back propagation (BP) neural network method optimized by the genetic algorithm (GA-BP) was proposed to set up the interface delamination thickness prediction model. As a result, the root correlation coefficient R^2 reached over 0.95, the various errors—including the mean square error, mean squared percentage error, and mean absolute percentage error—were less than or equal to 0.53. All these indicators proved that the trained hybrid SWT-PCA-GA-BP model had excellent prediction performance and high accuracy. Finally, this work proposed a novel and convenient interface delamination evaluation method that could also be potentially utilized to evaluate the structural integrity of TBCs.

Keywords: TBCs; terahertz technique; interface delamination; FDTD; SWT-PCA-GA-BP

1. Introduction

Aero-engine technology is known as the jewel in the industrial crown and is also the focus technology that countries all over the world are pursuing. The continuous improvement of the thrust-to-weight ratio puts forward higher challenges for the refractoriness and corrosion resistance of the hot-end components of aero-engines. Even though the most effective cooling structure technology is used, the extreme temperature of advanced superalloy material is still far from meeting the surface temperature of the turbine blade. Thermal barrier coatings (TBCs) have been widely used as a protective material for hot-end components of aero-engines, owing to their excellent high-temperature resistance, low thermal conductivity, and anti-wear and anti-corrosion properties, which can effectively improve

the working temperature and thrust-weight ratio of gas turbines [1,2]. The hot-end components are exposed to the harsh service environment of high-temperature oxidation, erosion impact, and high thermal fatigue for a long time. Beyond that, owing to the discrepancy in thermal expansion coefficient between superalloy substrate and ceramic top coat, phenomena such as thickness thinning, formation of the thermally grown oxide layer (TGO), and spalling have severely restricted the service life and reliability of TBCs under the action of thermal stress mismatch [3–5]. Previous studies have shown that the initiation, expansion, and merging of internal cracks are one of the most vital causes for the failure of TBCs [6,7]. Interface delamination generates under repeated high-temperature thermal shock cycles, owing to the crack propagation along the bottom of TBCs, and the interface delamination will induce the ceramic top coat to peel off and fail. Therefore, to ensure the structural integrity and life safety of aero-engine blades, it is urgent to effectively monitor the interface delamination of the thermal barrier coating in the early stage.

As shown in Table 1, traditional non-destructive testing methods—including ultrasonic waves, eddy current, X-rays, and infrared—cannot evaluate the interface delamination well. For example, owing to the existence of edge effects and the requirement of a liquid couplant, ultrasonic waves are limited to the size of the target object. Eddy current is not suitable for dielectric materials characterization. X-rays are high-radiation electromagnetic waves, in theory, it is more accurate than the terahertz measurement. Nevertheless, X-rays have a threat to human health and require additional protective devices. Moreover, high-dose X-rays are not only a threat to human health, but also have the risk of causing defects in the internal crystals of the TBCs. Not only that, X-rays are difficult to detect flat defects, such as cracks, delamination, and debonding. The infrared does not have the sufficient ability to penetrate the ceramic topcoat to distinguish the interface delamination [8–11]. Terahertz technology has been increasingly applied to the field of nondestructive testing as a new monitoring technology over recent years. Compared with traditional non-destructive testing methods, terahertz waves have strong penetrability to dielectric materials, and they can detect objects under low radiation, non-contact, and non-destructive conditions, and they have high detection accuracy without coupling, which is one of the important non-destructive testing research directions [12]. Terahertz non-destructive evaluation technology has been applied in various fields, mainly including human security, integrated circuits, biopharmaceuticals, glass fiber reinforced plastic materials and thermal barrier coatings, of which the research in thermal barrier coatings non-destructive evaluation mainly focuses on the detection and characterization of ceramic layer thickness [13,14], interface TGO [15,16], ceramic top coat microstructure features [17–19], and erosion morphology [20]. In the previous studies, much more attention was paid to the latter two, and it was found that terahertz technology is the only non-destructive testing method that combines safety, high precision and resolution of interface cracks. Therefore, it is considered that terahertz is more suitable for evaluating the TBCs delamination than X-rays. There are few reports about the terahertz nondestructive research on interface delamination evaluation of thermal barrier coatings.

Table 1. Comparison of detection capabilities of different thermal barrier coating nondestructive testing methods.

Methods	Detectable Content
Ultrasonic waves	Elasticity modulus, thickness, bond quality
Eddy current	Thickness, porosity
X-rays	Thickness, porosity, pore structure
Infrared	Thickness, crack, delamination, degradation
Terahertz	Thickness, porosity, TGO, microstructure feature, delamination

In this work, FDTD numerical simulation method was applied to obtain the terahertz time-domain signals of the TBCs samples with different interface delamination thickness. Nevertheless, the delamination signal was still very weak in terahertz time-frequency waveforms and the conventional

signal filtering and deconvolution approaches could not distinguish the slight interface delamination. The SWT method was employed to preprocess the raw terahertz time-domain signals and the PCA approach was used to reduce the data dimension of these terahertz time-domain signals processed by SWT. By using the hybrid artificial neural network algorithm, the optimization regression model was set up to predict the thickness of the interface delamination.

2. Simulations and Modeling

2.1. Terahertz Simulation Signal Obtained by FDTD Algorithm

As shown in Figure 1, the terahertz waves are incident on the surface of the TBCs, part of the terahertz waves will reflect back to the air in advance, part of the terahertz waves penetrate into the top coat, to reflect and transmit at the interface of delamination repeatedly. The interface delamination could be simplified as the ultrathin air layer inside the TBCs; in theory, the thickness information of the interface delamination could be extracted by analyzing the time difference between the multiple echoes. However, in practice, previous studies (including ours) [15,21] showed that it is very hard to extract the time difference (peak finding) to estimate the interface delamination thickness for the thicknesses in the range of ~100 microns; not only that, the peak finding method is difficult for field engineer.

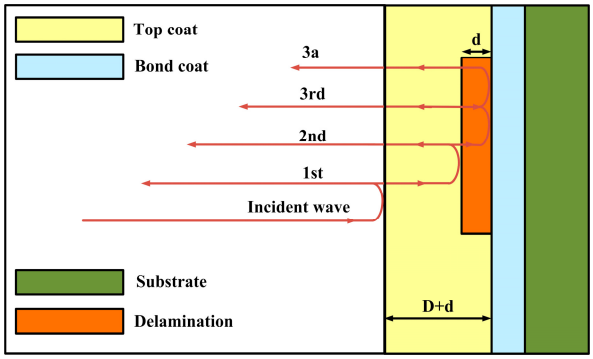


Figure 1. Schematic diagram of terahertz waves propagation path in the thermal barrier coatings with the interface delamination.

The ZrO_2 8 wt % Y_2O_3 (8YSZ) powder (15~45 μm, Beijing Sunspraying Technology Co., Ltd., Beijing, China) was employed to prepare the top coat (spray power: 36 kW, spray distance: 90 mm, power feed rate: 10 L/min, spray gun speed: 15 cm/s), as shown in Figure 2, the complex refractive index of the ceramic coat was tested using a TAS7400TS transmission terahertz time-domain spectroscopy system (Advantest Corporation, Tokyo, Japan). The wavelength was 1560 nm, the pulse width was 300 fs, and the frequency resolution was 1.9 GHz.

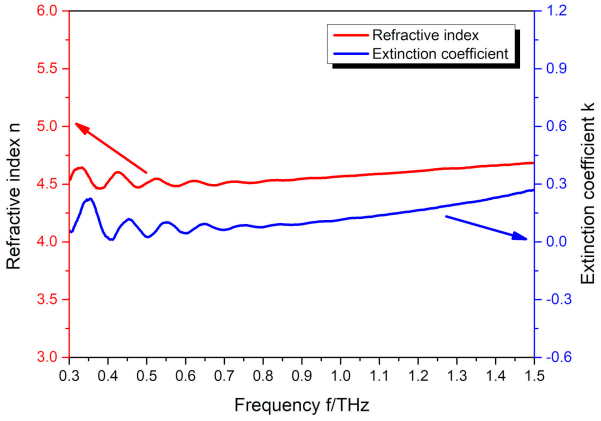


Figure 2. Complex refractive index of the top coat.

In this study, the FDTD Solutions software (Lumerical Solutions Inc., Vancouver, Canada) was applied to set up the simulation model and simulate the propagation process of terahertz waves in the TBCs with various thicknesses of top coat and interface delamination. The incident broadband terahertz Gaussian waves in the range of 0.3–1.5 THz were set vertical to the TBCs surface, the reflection echoes were recorded and analyzed for the TBCs interface delamination evaluation [22,23]. Perfectly matched layer (PML) boundary condition was set in the terahertz incidence Z direction, periodic boundary conditions were set in the X and Y directions, and the complex refractive index shown in Figure 2 was imported into the FDTD model as the terahertz property of ceramic top coat to mimic the actual detection process. As shown in Table 2, the influences of the top coat thickness, the interface delamination thickness, and the roughness are considered comprehensively for modeling and analysis. When setting up the FDTD model, the thickness of YSZ top coat ranges from 100~410 μm (interval: 10 μm) during modeling; the thickness of interface delamination ranges from 1~20 μm (eight kinds of thickness, each thickness occurs four times during modeling); the surface roughness of YSZ top coat ranges from 2~8 μm (four kinds of thickness, each thickness occurs eight times during modeling); the surface and bottom roughness of interface delamination also ranges from 2~8 μm (four kinds of thickness, each thickness occurs eight times during modeling). Hence, a total of 32 FDTD models is obtained and calculated.

Table 2. Parameter settings for the thickness and roughness.

Layer	Optional Thickness (μm)	Optional Roughness (R_a/μm)
YSZ top coat	100~410 (interval: 10)	2, 4, 6, and 8
Interface delamination	1, 3, 5, 8, 10, 12, 15, and 20	2, 4, 6, and 8

2.2. Data Processing and Feature Extraction

Wavelet transform technique was used to process the raw terahertz signals obtained by these FDTD models to extract the features. The scaling function $\varphi(x)$ and mother wavelets function $f(x)$ used in the wavelet transform can be expressed as [24,25]

$$2^{-\frac{1}{2}}\varphi\left(\frac{x}{2}-k\right)=\sum_{n=-\infty}^{+\infty}h(n-2k)\varphi(x-n) \tag{1}$$

$$2^{-\frac{1}{2}}f\left(\frac{x}{2}-k\right)=\sum_{n=-\infty}^{+\infty}g(n-2k)f(x-n) \tag{2}$$

here $h(n)$ and $g(n)$ are the impulse responses of low-pass filter and high-pass filter, respectively. Compared with the traditional discrete wavelet transform (DWT) algorithm, SWT is an up-sampling process by inserting zeros between each of the other filter coefficients, rather than down-sampling the signal. The decimation coefficient sequence is not performed at every stage, thus avoiding the translation variance and preserving the more detail signal. SWT decomposes the original signal $x(n)$ into the approximation coefficient vector $A_j(n)$ and the detail coefficient vector $D_j(n)$, and the data length is equal to the original signal length, the decomposition process is shown in Figure 3.

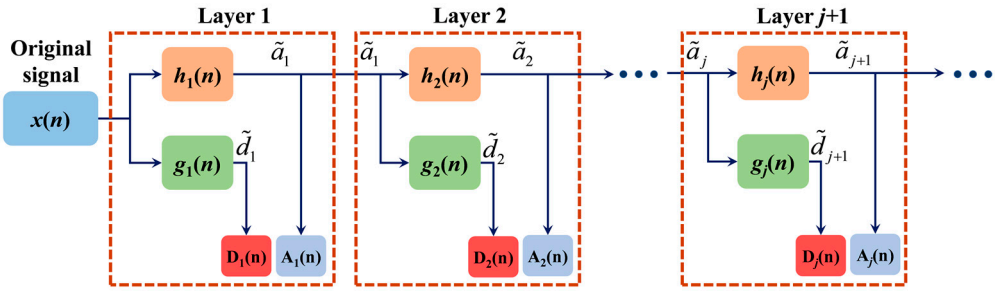


Figure 3. Schematic of the decomposition signal obtained by SWT.

The approximation coefficients mainly preserve the low-frequency information of the original signal, and the detail coefficients mainly preserve the high-frequency information of the original signal [26]. The approximation and detail coefficients at the jth layer can be computed by Equations (3) and (4) below, and the decomposition signal at the $(j + 1)$th layer can be estimated as

$$\tilde{a}_{j,k} = \left\langle f(t), \frac{1}{2^{j/2}} \varphi\left(\frac{t-k}{2^j}\right) \right\rangle \tag{3}$$

$$\tilde{d}_{j,k} = \left\langle f(t), \frac{1}{2^{j/2}} f\left(\frac{t-k}{2^j}\right) \right\rangle \tag{4}$$

$$\tilde{a}_{j+1,k} = \sum_{n=-\infty}^{+\infty} h(n) \tilde{a}_{j,k+2^j n} \tag{5}$$

$$\tilde{d}_{j+1,k} = \sum_{n=-\infty}^{+\infty} g(n) \tilde{d}_{j,k+2^j n} \tag{6}$$

here $f(t)$ is the original signal, k is a non-zero integer, $\varphi(\cdot)$ is the scale function, $f(\cdot)$ is the wavelet function, $\tilde{a}_{j,k}$ and $\tilde{d}_{j,k}$ are the approximation coefficients and detail coefficients at the jth layer, respectively.

In this work, based on the SWT, the original raw terahertz time-domain signals were decomposed into the approximation coefficients and detail coefficients. Previous studies showed that the detail coefficients were more suitable to be used to characterize the microscale features during modeling. In this work, the original terahertz data was decomposed at level 2 with the db1 mother wavelet, and the SWT detail data was applied to train the GA-BP network [27].

Principal component analysis (PCA) is an important statistical analysis approach to evaluate the correlation between multiple variables. Through linear transformation, the original data is transformed into a set of linearly independent representations of each dimension, and the main features of the data can be extracted as much as possible while retaining the original variable information as much as possible, and the weights can be calculated [17,28].

Suppose there are s samples, and each sample has b observation indicators. Original data could be expressed as

$$X = \begin{bmatrix} x_{11} & x_{12} \cdots & x_{1b} \\ x_{21} & x_{22} \ldots & x_{2b} \\ \vdots & \vdots & \ddots \\ x_{s1} & x_{s2} \cdots & x_{sb} \end{bmatrix} \tag{7}$$

here, b indicators form a b-dimensional random vector, $X = (X_1, X_2 \ldots X_b)$.

Standardize the data of each variable to eliminate the influence of dimension, the standardized data matrix is used to calculate the correlation coefficient matrix of the variables according to

$$r_{ij} = \frac{\sum_{q=1}^{s}\left(x_{qi}-\overline{x}_i\right)\left(x_{qj}-\overline{x}_j\right)}{\sqrt{\sum_{q=1}^{s}\left(x_{qi}-\overline{x}_i\right)^2\sum_{q=1}^{s}\left(x_{qj}-\overline{x}_j\right)^2}} \tag{8}$$

The standardized correlation coefficient matrix is expressed as

$$R_{ij} = \left(r_{ij}\right)_{b\times b} \tag{9}$$

On the basis of the equation $\left|R_{ij}-\lambda_j E\right| = 0$, the b characteristic roots λ_j of R_{ij} can be obtained. Then find the corresponding feature vector as

$$a_1 = \begin{bmatrix} a_{11} \\ a_{21} \\ \vdots \\ a_{b1} \end{bmatrix}, a_2 = \begin{bmatrix} a_{12} \\ a_{22} \\ \vdots \\ a_{b2} \end{bmatrix}, \quad \cdots, a_p = \begin{bmatrix} a_{1b} \\ a_{2b} \\ \vdots \\ a_{bb} \end{bmatrix} \tag{10}$$

The principal component could be expressed as

$$F_i = a_{1i}X_1 + a_{2i}X_2 + \cdots + a_{bi}X_b, \quad i = 1, \cdots b \tag{11}$$

The contribution rate of each principal component (PC) is estimated as

$$\frac{\lambda_i}{\Sigma_{q=1}^{b}\lambda_k}(i = 1, 2, \cdots b) \tag{12}$$

The cumulative contribution rate of PCs is estimated as

$$\frac{\sum_{q=1}^{i}\lambda q}{\sum_{q=1}^{b}\lambda q}(i = 1, 2, \cdots b) \tag{13}$$

To determine the number of principal components, generally take the first $l(l \leq b)$ PCs corresponding to the eigenvalues whose cumulative contribution rate reaches 85%.

In this study, the SWT and PCA function were implemented through MATLAB programming. The 32 sets of terahertz time-domain data were processed by SWT. After PCA processing, the contribution rate and the cumulative contribution rate were obtained. These PCs were used as the input features during modeling.

2.3. Hybrid Artificial Neural Network Model

The back propagation (BP) neural network is a multilayer feedforward neural network with complex pattern classification capability and excellent multi-dimensional function mapping capability. The BP neural network iterates on the weights and thresholds of neurons by the principle of back propagation, each iteration of weight and threshold will be adjusted toward the direction of the output error reduction [29–31]. The BP neural network formula could be expressed as

$$f(X) = W^T \bullet X + c \tag{14}$$

Here, X is the input matrix, W is the weighting matrix, and c is the threshold.

The BP neural network mainly contains an input layer, several hidden layers and an output layer. Generally, the triple-layer BP neural network has been able to solve complex nonlinear mapping problems [29,30]. In this work, as shown in Figure 4, the triple-layer BP neural network is applied to set up the prediction model. The minimum error of the training target is set to 0.01, the number of trainings is 1000, and the two transfer functions are respectively set to "tansig" and "logsig".

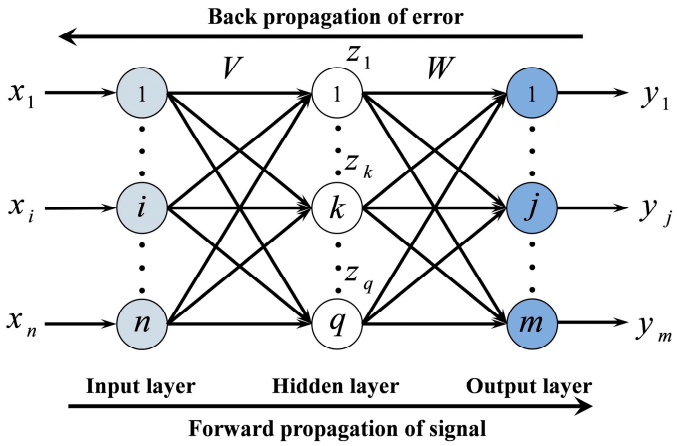


Figure 4. Structure of triple-layer BP neural network.

The genetic algorithm (GA) is an approach designed to seek for the optimal solution by simulating the natural evolutionary process. When solving more complicated assorted optimization problems, it is usually applied to acquire better results faster than other algorithms [32,33].

Although the BP neural network can solve complex nonlinear mappings, its prediction performance will be affected by the initial weight and threshold, resulting in a large gap in the prediction performance of multiple training. Therefore, as shown in Figure 5, GA is applied to optimize the initial values and the detailed execution steps are as follows [34–36]:

- Determine the basic structure of BP neural network, including the number of the input neurons, the hidden neurons, the output neurons, and the hidden layers.
- Encoding. The formula for calculating the length of the code can be expressed as

$$S = S_{input} \times S_{hidden} + S_{hidden} \times S_{output} + S_{hidden} + S_{output} \quad (15)$$

  where S is the code length, S_{input}, S_{hidden} and S_{output} are the input neuron number, hidden neuron number and output neuron number, respectively.
- Design the degree of fitness function. The fitness function is employed to measure the merit degree. In this work, the degree of fitness function was designed based on the prediction index mean squared error.
- Define the genetic algorithm parameters and initialize the population. The optimization algorithm parameters include the population size, the iteration number, the variation probability, and the crossover probability.
- Estimate the fitness value of the population according to the fitness function designed in Step (3).
- Use the fitness value as the basis for selection, crossing, and variation of the population. If the termination condition is met, the calculation is terminated; if not, return back to Step (5) until the termination condition is achieved.
- Decode the optimal individuals in the population as initial weights and thresholds and train the BP model.
- Test the BP model performance after training completion.

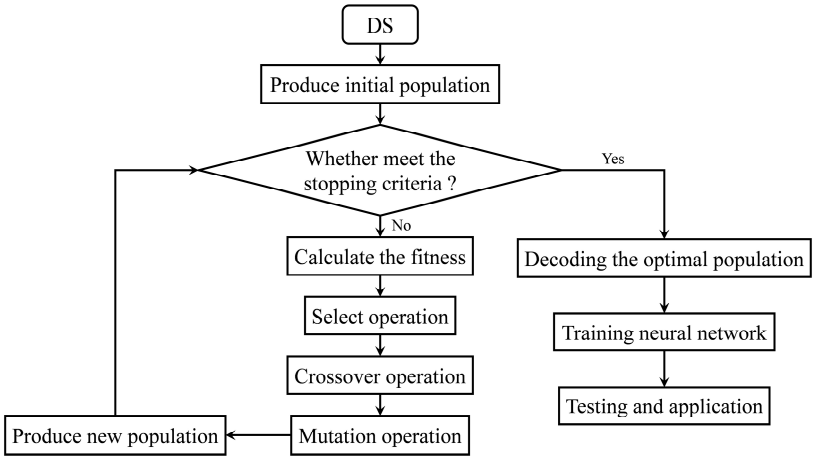


Figure 5. Calculation flow of GA-BP algorithm.

In this work, the prediction accuracy and reliability of the GA-BP algorithm were estimated via four parameters: root correlation coefficient (R^2), mean squared error (MSE), mean squared percentage error (MSPE), and mean absolute percentage error (MAPE). Their definitions can be expressed as

$$R^2 = \left(\sum_{i=1}^{m}\left(\hat{Y}_i - \overline{\hat{Y}}\right)\left(Y_i - \overline{Y}\right)\right) / \sqrt{\sum_{i=1}^{m}\left(\hat{Y}_i - \overline{\hat{Y}}\right)^2} \sqrt{\sum_{i=1}^{m}\left(Y_i - \overline{Y}\right)^2}^{2} \quad (16)$$

$$MSE = \sqrt{\sum_{i=1}^{m}\left|Y_i - \hat{Y}_i\right|^2} / m \quad (17)$$

$$MSPE = \sqrt{\sum_{i=1}^{m}\left(\left|Y_i - \hat{Y}_i\right| / Y_i\right)^2} / m \quad (18)$$

$$MAPE = \sum_{i=1}^{m} \frac{\left|Y_i - \hat{Y}_i\right|}{Y_i} / m \quad (19)$$

here m is the number of samples, Y_i is the actual value of interface delamination thickness, $\hat{Y}_i$ is the predicted value of interface delamination thickness obtained by GA-BP model.

3. Results and Discussion

As shown in Figure 6, for instance, the terahertz time-domain signals of sample 1 and sample 16 obtained by FDTD calculation and SWT processing are compared with each other. Comparison results show that both the variations of the thickness and the roughness will lead to the change of the time-domain wave on the amplitude and the optical delay, owing to the existence of interface delamination, the ideal time differences for the delamination thickness 1 and 20 μm depicted in Figure 6 should be 0.0067 and 0.1333 ps, respectively. If the peak finding method is applied to estimate the delamination thickness, it is nearly impossible. Nevertheless, SWT detail coefficients have kept the main characteristic peak position unchanged and also played the role of waveform baseline adjustment. Hence, the SWT approach has the potential to assist a machine learning model to distinguish the thin interface delamination layer and previous studies had proven its effectiveness [15,22].

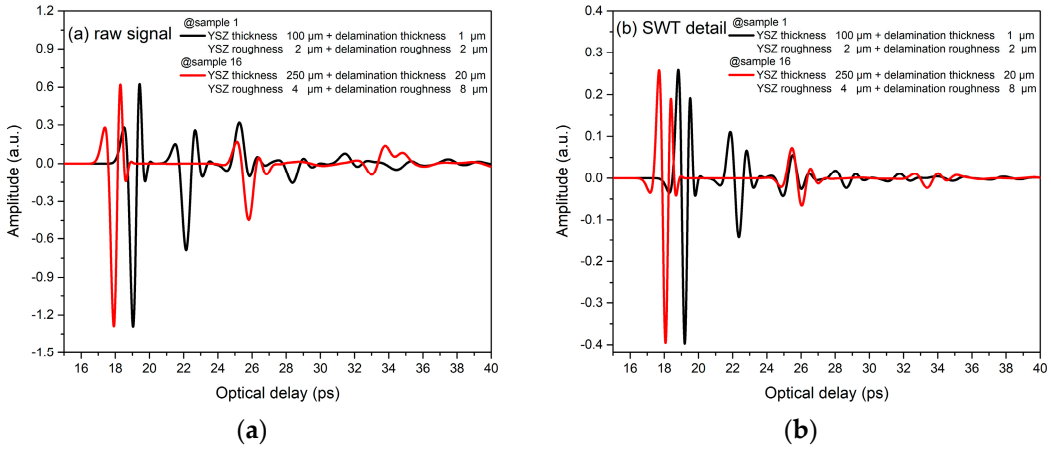


Figure 6. Terahertz time domain signals of sample 1 and sample 16: (**a**) raw signal; (**b**) SWT detail signal.

As shown in Figure 7, to make the cumulative contribution rate reach 100%, it is found that the cumulative contribution rate of the first 31 PCs of the SWT detail data. Finally, the data dimension is reduced from 32 × 3840 to 32 × 31, these dimension-reduced data are used as the input for the BP and GA-BP models to evaluate the interface delamination thickness.

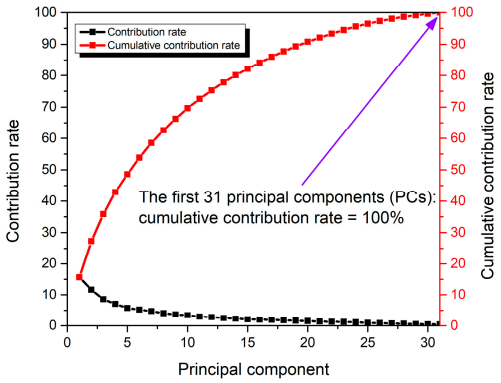


Figure 7. Contribution rate of each PC and their cumulative contribution rate of the PCs.

As shown in Figure 8, the GA-BP model is trained by selecting twenty-six random data sets, it could be seen from the fitness evolution curve that the training error of the parameter reached the minimum value and fulfilled the trained requirement when the training model evolved to the 433 generations, respectively.

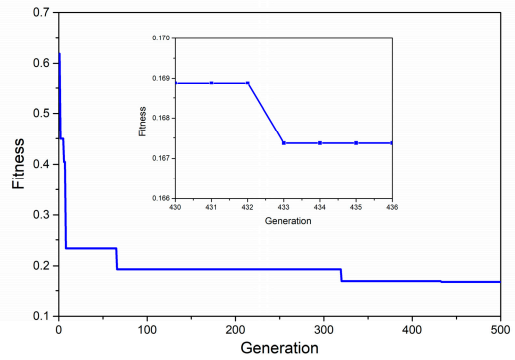


Figure 8. Fitness evolution curve of the thickness of interface delamination.

To compare and test the prediction accuracies and reliabilities of the simple BP and the hybrid GA-BP models, their performances are verified via the remaining six random samples. As shown in Figure 9, the black, green, and red symbols represent the actual, BP predicted, and GA-BP predicted values of the thickness of interface delamination, and the results show that the variation trend of their prediction results is basically consistent with each other.

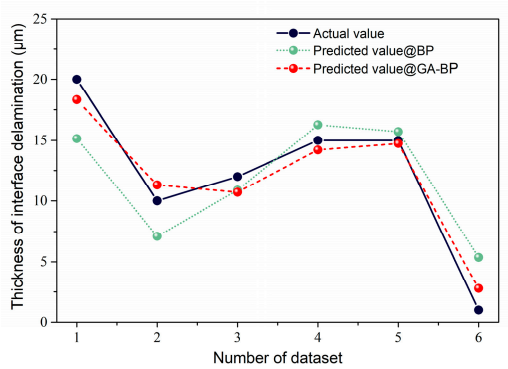


Figure 9. Prediction results of the interface delamination thickness of the BP and GA–BP regression model.

For the sake of further comparison between the BP and GA-BP models, as shown in Table 3, their accuracies and reliabilities could be seen clearly, the R^2 value of the GA-BP model has reached over 0.95, which is greater than the R^2 value of the BP model; the values of all these error performance indicators (MSE, MSPE, MAPE) of the GA-BP model are kept very low (≤0.5300), which are lower than the various errors of the BP model (≥1.8636). All these proved that the GA-BP model showed the higher accuracy and reliability in predicting the thickness of interface delamination; hence, the hybrid GA-BP algorithm model could satisfy the needs of in actual interface delamination evaluation.

Table 3. Prediction performance of the BP and GA-BP models tested by the six remaining random samples.

Prediction Results	R^2	MSE	MSPE	MAPE
BP	0.7370	2.9291	1.8636	2.1833
GA-BP	0.9511	0.5300	0.3011	0.3647

4. Conclusions

In this study, the terahertz nondestructive technology combined with the hybrid machine learning algorithm was applied to estimate the thickness of the interface delamination in the early stage. Major and useful conclusions are summarized as follows:

- It was found that FDTD model could be used to simulate the propagation process of terahertz waves in the TBCs with various thicknesses of interface delamination. The simulated terahertz time-domain signals after SWT processing showed that the detail coefficient kept the main characteristic peak position of raw signals and also adjusted waveform baseline.
- The PCA approach could be effectively used to reduce the SWT data dimension to improve the computational speed during modeling, the top 31 PCs were chosen instead of the original SWT signals as the input data during machine learning modeling, owing to their cumulative contribution rate (100%).
- To get the prediction accuracy and reliability of the BP model improved, the GA algorithm was employed to optimize the BP model. Finally, the hybrid SWT-PCA-GA-BP regression model with high R^2 value (>0.95) and low error values (≤0.5300) were obtained, the hybrid SWT-PCA-GA-BP model showed its high accuracy and reliability in predicting the thickness of interface delamination,

hence, it could be potentially used to monitor the TBCs delamination progression starting from the early stage of subcritical delamination crack propagation.

- Additionally, this novel terahertz nondestructive technology combined hybrid artificial neural network would be potentially applied in the future to monitor and improve the service life of TBCs.

Author Contributions: Data curation, D.Y., Z.X., H.F., J.H., and Y.L.; formal analysis, D.Y.; funding acquisition, W.W.; investigation, D.Y., C.Y., Z.X., H.F., J.H., and Y.L.; methodology, D.Y., W.W., and C.Y.; software, D.Y., C.Y., and Z.X.; supervision, W.W.; validation, D.Y.; writing—original draft, D.Y.; writing—review and editing, W.W. All authors have read and agreed to the published version of the manuscript.

Funding: This research was funded by National Natural Science Foundation of China (No. 51775189) and Science and Technology Commission of Shanghai Municipality Project (No. 16DZ2260604).

Conflicts of Interest: The authors declare no conflict of interest.

References

1. Padture, N.P.; Gell, M.; Jordan, E.H. Thermal barrier coatings for gas-turbine engine applications. *Science* **2002**, *296*, 280–284. [CrossRef] [PubMed]
2. Nicholls, J.R. Advances in coating design for high-performance gas turbines. *MRS Bull.* **2003**, *28*, 659–670. [CrossRef]
3. Kumar, V.; Balasubramanian, K. Progress update on failure mechanisms of advanced thermal barrier coatings: A review. *Prog. Org. Coat.* **2016**, *90*, 54–82. [CrossRef]
4. Giolli, C.; Scrivani, A.; Rizzi, G.; Borgioli, F.; Lusvarghi, L. Failure mechanism for thermal fatigue of thermal barrier coating systems. *J. Therm. Spray Technol.* **2009**, *18*, 223–230. [CrossRef]
5. Hutchinson, J.W.; Evans, A.G. On the delamination of thermal barrier coatings in a thermal gradient. *Surf. Coat. Technol.* **2002**, *149*, 179–184. [CrossRef]
6. Lv, J.N.; Fan, X.L.; Li, Q. The impact of the growth of thermally grown oxide layer on the propagation of surface cracks within thermal barrier coatings. *Surf. Coat. Technol.* **2017**, *309*, 1033–1044. [CrossRef]
7. Song, D.; Song, T.; Paik, U.; Lyu, G. Crack-growth behavior in thermal barrier coatings with cyclic thermal exposure. *Coatings* **2019**, *9*, 365. [CrossRef]
8. Chen, H.-L.R.; Zhang, B.; Alvin, M.A.; Lin, Y. Ultrasonic detection of delamination and material characterization of thermal barrier coatings. *J. Therm. Spray Technol.* **2012**, *21*, 1184–1194. [CrossRef]
9. Yong, L.; Chen, Z.; Mao, Y.; Yong, Q. Quantitative evaluation of thermal barrier coating based on eddy current technique. *NDT E Int.* **2012**, *50*, 29–35. [CrossRef]
10. Queralt, I.; Ibañez, J.; Marguí, E.; Pujol, J. Thickness measurement of semiconductor thin films by energy dispersive X-ray fluorescence bench-top instrumentation: Application to GaN epilayers grown by molecular beamepitaxy. *Spectroc. Acta Part B At. Spectrosc.* **2010**, *65*, 583–586. [CrossRef]
11. Shrestha, R.; Kim, W. Evaluation of coating thickness by thermal wave imaging: A comparative study of pulsed and lock-in infrared thermography—Part II: Experimental investigation. *Infrared Phys. Technol.* **2018**, *92*, 24–29. [CrossRef]
12. Zhong, S. Progress in terahertz nondestructive testing: A review. *Front. Mech. Eng.* **2018**, *14*, 273–281. [CrossRef]
13. Fukuchi, T.; Fuse, N.; Fujii, T.; Okada, M. Topcoat thickness measurement of thermal barrier coating of gas turbine blade using terahertz wave. *Electr. Eng. Jpn.* **2014**, *189*, 1–8. [CrossRef]
14. Fukuchi, T.; Fuse, N.; Fujii, T.; Okada, M. Measurement of refractive index and thickness of topcoat of thermal barrier coating by reflection measurement of terahertz waves. *Electron. Commun. Jpn.* **2013**, *96*, 37–45. [CrossRef]
15. Luo, M.; Zhong, S.; Yao, L.; Tu, W.; Nsengiyumva, W.; Chen, W. Thin thermally grown oxide thickness detection in thermal barrier coatings based on SWT-BP neural network algorithm and terahertz technology. *Appl. Opt.* **2020**, *59*, 4097–4104. [CrossRef] [PubMed]
16. Chen, C.C.; Lee, D.J.; Pollock, T.; Whitaker, J.F. Pulsed-terahertz reflectometry for health monitoring of ceramic thermal barrier coatings. *Opt. Express* **2010**, *18*, 3477–3486. [CrossRef]
17. Ye, D.; Wang, W.; Zhou, H.; Fang, H.; Huang, J.; Li, Y.; Gong, H.; Li, Z. Characterization of thermal barrier coatings microstructural features using terahertz spectroscopy. *Surf. Coat. Technol.* **2020**, *394*, 125836. [CrossRef]

18. Ye, D.; Wang, W.; Zhou, H.; Huang, J.; Wu, W.; Gong, H.; Li, Z. In-situ evaluation of porosity in thermal barrier coatings based on the broadening of terahertz time-domain pulses: Simulation and experimental investigations. *Opt. Express* **2019**, *27*, 28150–28165. [CrossRef]
19. Ye, D.; Wang, W.; Zhou, H.; Li, Y.; Fang, H.; Huang, J.; Gong, H.; Li, Z. Quantitative determination of porosity in thermal barrier coatings using terahertz reflectance spectrum: Case study of atmospheric-plasma-sprayed YSZ coatings. *IEEE Trans. Terahertz Sci. Technol.* **2020**, *10*, 383–390. [CrossRef]
20. Ye, D.; Wang, W.; Huang, J.; Lu, X. Nondestructive interface morphology characterization of thermal barrier coatings using terahertz time-domain spectroscopy. *Coatings* **2019**, *9*, 89. [CrossRef]
21. Ye, D.; Wang, W.; Zhou, H.; Fang, H.; Huang, J.; Gong, H.; Li, Z. Parallel crack monitoring of thermal barrier coatings based on terahertz technology. *Surf. Technol.* **2020**, *49*, 91–97.
22. Tu, W.; Zhong, S.; Shen, Y.; Atilla, I.; Fu, X. Neural network-based hybrid signal processing approach for resolving thin marine protective coating by terahertz pulsed imaging. *Ocean Eng.* **2019**, *173*, 58–67. [CrossRef]
23. Sullivan, D.M. *Electromagnetic Simulation Using the FDTD Method*; IEEE Press: Piscataway, NJ, USA, 2013.
24. Mortazavi, S.H.; Shahrtash, S.M. Comparing denoising performance of DWT, WPT, SWT and DT-CWT for partial discharge signals. In Proceedings of the 43rd International Universities Power Engineering Conference, Padova, Italy, 1–4 September 2008; pp. 1–6.
25. Jamaluddin, F.N.; Ahmad, S.A.; Noor, S.B.M.; Hassan, W.Z.W.; Yaacob, A.; Adam, Y. Performance of DWT and SWT in muscle fatigue detection. *Biomed. Eng. Sci. IEEE* **2015**, 50–53. [CrossRef]
26. Dong, J.; Locquet, A.; Citrin, D.S. Enhanced terahertz imaging of small forced delamination in woven glass fibre-reinforced composites with wavelet de-noising. *J. Infrared Millim. Terahertz Waves* **2015**, *37*, 289–301. [CrossRef]
27. Brychta, R.J.; Tuntrakool, S.; Appalsamy, M.; Keller, N.R.; Roberson, D.; Shiavi, R.G.; Diedrich, A. Wavelet methods for spike detection in mouse renal sympathetic nerve activity. *IEEE Trans. Biomed. Eng.* **2007**, *54*, 82–93. [CrossRef]
28. He, F.; Zhang, L. Prediction model of end-point phosphorus content in BOF steelmaking process based on PCA and BP neural network. *J. Process Control* **2018**, *66*, 51–58. [CrossRef]
29. Guo, Z.H.; Wu, J.; Lu, H.Y.; Wang, J.Z. A case study on a hybrid wind speed forecasting method using bp neural network. *Knowl.-Based Syst.* **2011**, *24*, 1048–1056. [CrossRef]
30. Ren, C.; An, N.; Wang, J.; Li, L.; Hu, B.; Shang, D. Optimal parameters selection for bp neural network based on particle swarm optimization: A case study of wind speed forecasting. *Knowl.-Based Syst.* **2014**, *56*, 226–239. [CrossRef]
31. Ma, L.; Wang, B.; Yan, S.; Gu, X. Temperature error correction based on bp neural network in meteorological wireless sensor network. *Int. J. Sens. Netw.* **2016**, *23*, 265. [CrossRef]
32. Ehyaei, M.A.; Rosen, M.A. Optimization of a triple cycle based on a solid oxide fuel cell and gas and steam cycles with a multi-objective genetic algorithm and energy, exergy and economic analyses. *Energy Convers. Manag.* **2019**, *180*, 689–708. [CrossRef]
33. Salah, B.; Ali, F.; Ali, O.; Mohamed, S. Optimal deep learning LSTM model for electric load forecasting using feature selection and genetic algorithm: Comparison with machine learning approaches. *Energies* **2018**, *11*, 1636.
34. Wang, S.; Zhang, N.; Wu, L.; Wang, Y. Wind speed forecasting based on the hybrid ensemble empirical mode decomposition and ga-bp neural network method. *Renew. Energy* **2016**, *94*, 629–636. [CrossRef]
35. Yu, F.; Xu, X. A short-term load forecasting model of natural gas based on optimized genetic algorithm and improved bp neural network. *Appl. Energy* **2014**, *134*, 102–113. [CrossRef]
36. Zheng, D.; Qian, Z.D.; Liu, Y.; Liu, C.B. Prediction and sensitivity analysis of long-term skid resistance of epoxy asphalt mixture based on ga-bp neural network. *Constr. Build. Mater.* **2018**, *158*, 614–623. [CrossRef]



© 2020 by the authors. Licensee MDPI, Basel, Switzerland. This article is an open access article distributed under the terms and conditions of the Creative Commons Attribution (CC BY) license (http://creativecommons.org/licenses/by/4.0/).